RAPID COMMUNICATIONS IN MASS SPECTROMETRY, VOL. 9, 829–836 (1995)

Thermal Decomposition Kinetics of Protonated Peptides and Peptide Dimers, and Comparison with Surface-induced Dissociation

Michael Meot-Ner (Mautner),* Ashok R. Dongré, Árpád Somogyi,† Vicki H. Wysocki
Department of Chemistry, Virginia Commonwealth University, Richmond, VA 23284-2006, USA

Rate constants for the unimolecular decomposition of peptide monomer and dimer ions by thermal and surface-induced dissociation (SID) are measured and compared. Rate constants for thermal dissociation are measured in a heated wide-bore capillary flow reactor attached in front of the capillary leading into the mass spectrometer. Thermal decomposition of the leucine enkephalin ion (YGGFL)H^+ is observed between 600 and 680 K with rate constants of 20–200 s^{-1}, and yields many of the same fragments as SID at 35 eV, although with different relative intensities. The thermal decomposition yields the Arrhenius parameters $E_a = 38.3$ kcal/mol, log A = 15.7. The decomposition of the monomer and dimer ions are also observed by using SID on C_{18} and fluorinated hydrocarbon surfaces, with rate constants of 2×10^4 to 40×10^4 s^{-1}. The SID activated monomer ions are assigned equivalent temperatures of 710–840 K by extrapolation of the thermal activation parameters. The protonated dimer ion $(YGGFL)_2 H^+$ decomposes thermally at 500–540 K to yield the monomer ion. The dimer also decomposes by SID at low collision energies 10–20 eV on both surfaces to yield the monomer ion, and at much higher energies of 60–80 eV to yield fragments identical to the decomposition of the monomer. The large energy requirement for fragmentation from the dimer is due to energy deposition into more degrees of freedom plus the additional energy required for dissociation of the dimer to the monomer. It is assumed that the energy deposition is linear with collision energy up to 80 eV, and that the energy becomes randomized throughout the dimer, including energy flow through the hydrogen bond(s). These mechanistic assumptions are supported quantitatively by the SID energy relations between monomer and dimer fragmentation. Thermal decomposition of the larger, multiply protonated melittin ion $[M+3H]^{3+}$ occurs at substantially higher temperatures, between 810–840 K, than those required for thermal decomposition of (YGGFL)H^+, to yield many of the same sequence ions as produced by SID at 135 eV on a fluorinated surface.

The fragmentation of molecular ions or protonated molecules is essential for mass spectrometric structure determination, while the decomposition of gas-phase adducts may allow the determination of non-covalent binding energies. We previously studied the thermal decomposition kinetics of carbonium ions and protonated alcohols and ethers,[1–4] and the thermal decomposition of non-covalent, hydrogen-bonded dimers is observed routinely in the reverse processes of clustering equilibria. This work extends unimolecular kinetics to larger biomolecules. A similar application was presented more recently by Busman *et al.* for the decomposition of melittin ions.[5] The present work also extends previous work of the authors in ion pyrolysis and surface-induced dissociation (SID) to compare the energetics of these two processes.

Surface-induced dissociation, developed originally by Cooks and coworkers,[6] has proved to be a powerful technique for the investigation of the mass spectral fragmentation of protonated peptides.[7–13] In addition to practical applications, e.g. sequencing peptides, SID has the potential to provide energetic data that can be used to describe the mechanisms of peptide fragmentation. We have recently reported, for example, that fragmentation efficiencies (% fragmentation vs. collision energy) can be correlated with the basicities of peptides and with peptide size.[13] Although these qualitative trends are themselves important, it is desirable to further investigate the physico-chemical meaning of the fragmentation efficiency curves.

A critical consideration for correlating the position of the fragmentation efficiency curves with 'stabilities' is that we have no direct measure of the energy deposition to large biomolecules upon ion–surface collisions. For smaller ions, such as the molecular ions of $W(CO)_6$,[14,15] ferrocene[16] and benzene,[17] the kinetic energy–internal energy conversion can be predicted based on either the thermometer molecule method[18] or on the modified deconvolution method.[17] The published values are quite similar, although they show some differences depending on the projectile ion and the method used. For example, it was found for $W(CO)_6^+$ that alkanethiolate monolayers provide about 12% kinetic energy–internal energy transfer (which is comparable to the value of 11% reported for stainless steel,[15] and that fluorinated alkanethiolate monolayers provide much more effective conversion (19%).[14] On the other hand, the following values were reported for ferrocene[16] (24% on a fluorinated surface and 15% on an alkanethiolate surface) and benzene[17] (28% on a fluorinated surface and 17% on an alkanethiolate surface). The conversion values obtained for smaller molecular ions cannot be automatically transferred to larger protonated oligopeptides, although the relative differences in energy deposition (with surface type) are the same for peptides and these smaller molecules.[13b]

An ultimate goal of this research is to develop an approach that can be used to measure the kinetic energy–internal energy conversion upon collisions of protonated peptides with self-assembled monolayer

* Author for correspondence.
† On leave from the Central Research Institute for Chemistry of the Hungarian Academy of Sciences, PO Box 17, Budapest, Hungary.

CCC 0951–4198/95/090829–08

Received 22 May 1995
Accepted (revised) 7 June 1995

surfaces. As the first step toward this goal, in this paper we examine quantitatively the kinetics of decomposition of the molecular ion of a model peptide, protonated leucine enkephalin $(YGGFL)H^+$ and its dimer ion $(YGGFL)_2H^+$ (note that in the discussion below the dimer ion always refers to the protonated dimer ion), using both thermal dissociation and surface-induced dissociation (SID). Furthermore, we correlate the thermal and SID results by extrapolating the thermal dissociation parameters to obtain energetic information on the SID activated ions. The kinetics and energetics of the decompositions are of interest not only for mass spectrometry, but also because of their relation to the thermal stabilities and non-covalent binding energies of biopolymers.

RESULTS AND DISCUSSION

Surface-induced dissociation

Three different but interrelated dissociation processes were investigated: dissociation of the dimer $(YGGFL)_2H^+$ to protonated and neutral monomers of leucine enkephalin; dissociation of the monomer ion $(YGGFL)H^+$ to fragments; and dissociation from the dimer $(YGGFL)_2H^+$ to fragments of the monomer $(YGGFL)H^+$. It is expected that the latter process is shifted to higher energies because the internal energy deposited upon ion–surface collision is distributed among more degrees of freedom, and because energy is required to dissociate first the dimer into monomers, before further fragmentation occurs. We will now examine the results and the energy relationships between these processes.

Surface-induced dissociation spectra obtained by 70 eV collisions of $(YGGFL)_2H^+$ dimer and 30 eV collisions of $(YGGFL)H^+$ with the octadecanethiolate (C_{18}) are shown in Fig. 1(a) and (b), respectively. Both spectra contain practically the same ions with similar intensity patterns. There are no fragment ions in the range of m/z 560–1100 in the dimer SID spectrum (not shown in Fig. 1(a)). This indicates that the dimer dissociates first to monomer and protonated monomer, without losing small neutral species, and this process is followed by the fragmentation of the protonated monomer ions. This mechanism is also supported by the energy relationships below.

To perform a more detailed study, fragmentation efficiency curves[13] have also been determined for both the protonated dimer and protonated monomer of leucine enkephalin on two different self-assembled monolayer surfaces: perfluorooctyl-ethane thiolate surface (F-surface) and an octadecanethiolate surface (C_{18}-surface) (see Fig. 2(a) and (b)). The dimer $(YGGFL)_2H^+$ dissociates to the protonated monomer at low collision energies, with inflection points at 11 eV and 14 eV on the F and C_{18}-surfaces, respectively. At these energies, the only significant products are the monomer ions, $(YGGFL)H^+$. This is true even at higher energies, up to 50 eV on the C_{18} surface. There is a significant energy gap between the dissociation of the dimer to monomer and that of the further fragmentation from the dimer to fragments of the monomer. In fact, further fragmentation from the dimer is also shifted to much higher energies than fragmentation from the mass selected monomer. These energy shifts are shown by inflection points of the fragmentation

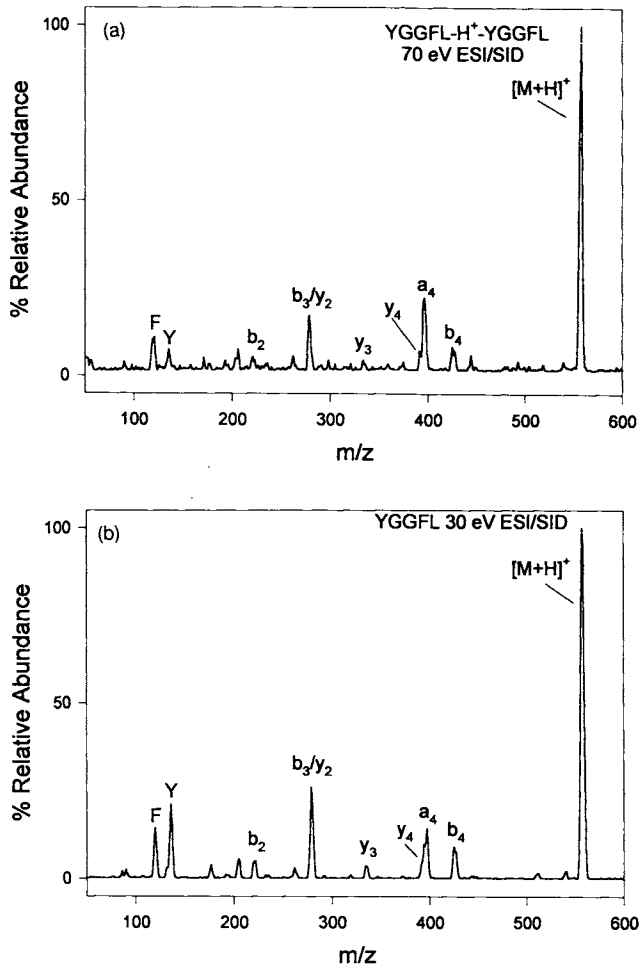

Figure 1. Surface-induced dissociation (SID) spectra obtained by (a) 70 eV collisions of $(YGGFL)_2H^+$ dimer (m/z region beyond 600 is not shown as there are no fragments observed) and (b) 30 eV collisions of $(YGGFL)H^+$ with the octadecanethiolate (C_{18}) surface.

efficiency curves as summarized in Table 1. On the C_{18} surface, the inflection points are 14.1 eV for $(YGGFL)_2H^+ \rightarrow (YGGFL)H^+ + YGGFL$; 27.3 eV for $(YGGFL)H_+ \rightarrow$ fragments; and 67.6 eV for $(YGGFL)_2H^+ \rightarrow$ fragments. The corresponding values for the fluorinated surface are 11.4, 13.4 and 40.8 eV, respectively.

The observed energy relationships can be justified on the basis of the following mechanistic assumptions.

(i) The dimer A_2H^+ collides with a surface and a fraction of the collision energy is deposited into the dimer ion at atoms or groups that directly interact with the surface. The deposited energy is directly proportional to the collision energy over the entire range studied (for the validity of this assumption, see, for example, Refs 14–17).

(ii) The internal energy is randomized throughout the entire dimer. Specifically, the energy is distributed between the monomer units statistically.

(iii) The protonated dimer dissociates to the monomer units, one of which is a neutral species and is unavailable for mass spectrometric investigations. Some of the internal energy is used for the dissociation of the dimer, but the remaining energy is statistically distributed to the charged and neutral monomers.

(iv) The protonated monomer unit further dissociates

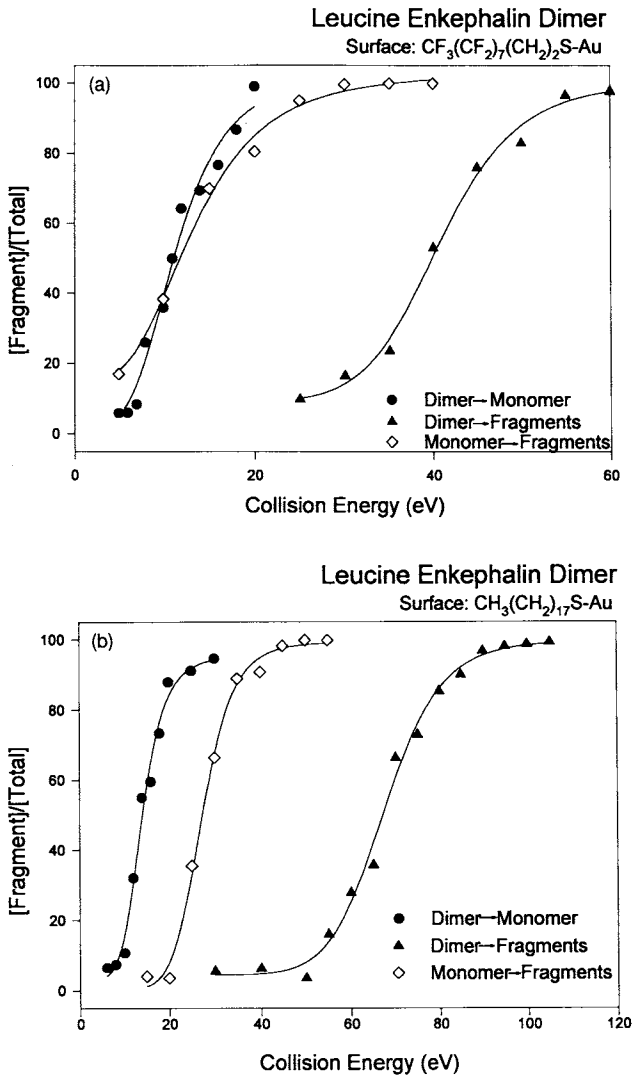

Figure 2. Fragmentation efficiency curves obtained for $(YGGFL)H^+$ monomer and $(YGGFL)_2H^+$ dimer on the (a) 2-perfluorooctylethanethiolate (F) surface and (b) octadecanethiolate (C_{18}) surface.

to its fragments. (The neutral component may also decompose but, as was mentioned above, this process is not observable in our experiments.)

Based on these processes, the energy deposition required to obtain low mass fragments from the dimer must provide energy to dissociate the dimer and leave the protonated monomer with enough energy for fragmentation even after the partitioning of the energy between the components. In other words, the energy deposited must be equal to the energy for dimer dissociation plus twice the energy required for fragmentation of the monomer (as half of the remaining energy will be carried away by the neutral monomer). An energy relationship accounting for total internal energy can be suggested as follows:

$$E_{(A_2H^+\rightarrow F^+)} = E_{(A_2H^+\rightarrow AH^+)} + 2E_{(AH^+\rightarrow F^+)}$$

40.8 $\approx$ 11.4 $+ 2\times(13.4)$, for the F surface.

67.6 $\approx$ 14.1 $+ 2\times(27.3)$, for the C_{18} surface.

If the kinetic energy–internal energy conversion is linear with the collision energy, the internal energies in Eqn (1) should be satisfied by entering the inflection point values from Fig. 1(a) and (b) as shown under the equations. Eqn (1) incorporates assumptions (i)–(iv) above, and since it is valid for the experimental data, this constitutes experimental support for these assumptions.[19]

An important implication is that the energy is being randomized in the entire dimer before decomposition to monomers. Therefore, the excess energy is randomized by flowing through the weak hydrogen bond or bonds that hold the complex together, before these weak bonds cleave. This applies even in the presence of the large excess energy required for further fragmentation of the monomer units. The probability of energy randomization without hydrogen bond breakage would be enhanced if the complex is bonded by several hydrogen bonds, as may be expected in a polyfunctional system. This would reduce substantially the probability that the hydrogen bonds break simultaneously, and therefore reduce the dissociation rate constant of the dimer ion.

The generality of Eqn (1) remains to be investigated. For example, preliminary studies on leucine enkephalin · · · leucine enkephalin arginine (mixed) dimer show it obeys an energy relationship similar to Eqn (1), but the fragmentation of the dimer of a small amino acid derivative (*N*-acetyl-alanin-methylester) does not, suggesting possibly decomposition without energy randomization. Further studies of the SID mechanism in various multimers, including multiply charged and specifically bonded adducts, are in progress.[20]

Thermal dissociation

For comparison with the SID energetics, we examined the thermal dissociation of $(YGGFL)H^+$ in a heated tube reactor. To obtain valid thermal unimolecular kinetics at the high pressure limit,[21] it is necessary that (i) the ion population be thermalized; (ii) the rate of activating collisions with the carrier gas be significantly greater than the rate of dissociation; and (iii) the carrier gas itself be thermally equilibrated with the reactor walls. To facilitate these conditions, the solution was electrosprayed into a wide-bore reactor tube, before passing into the capillary leading into the mass spectrometer. The advantages of such a reactor are: (i) because it has a higher gas conductance than the entry capillary, the pressure drop in the pre-capillary reactor is negligible, and the reactions occur at a well-defined pressure, within 10% of 1 atm in our set-up; (ii) since the mass flow through the reactor/capillary system is constant, the flow velocity is proportional to r^{-2}. For example, at our mass flow rate of $Q = 1\,Pa^3\,m^{-1}\,s$, at $P = 10^5$ Pa, the flow velocity in a reactor capillary with $r = 3.6\times10^{-4}$ m is 24 m s^{-1}, and the ion residence time in an 8 cm reactor zone is 3.4×10^{-3} s. Because of the r^{-2} dependence, the residence time is readily varied by using flow reactors with various radii, although the ion signal decreases at long residence times (large r) due to ion losses. We observed usable signal with r from 2×10^{-4} to 2×10^{-3} m, varying the residence time in an 8 cm reactor zone from 0.001 to 0.1 s. This brackets the measurable decomposition rate constants to the range of 4–400 s^{-1}. In comparison, with typical ion–molecule collision rate constants of $10^{-9}\,cm^3\,s^{-1}$ at 1 atm, the collision rate with the carrier gas, air, is $2.7\times10^{10}\,s^{-1}$. Therefore, the thermalizing collision rate is much

Table 1. Kinetic parameters for the thermal and surface-induced dissociation of protonated leucine enkephalin (MH^+) and protonated leucine enkephalin dimer (M_2H^+)

	Thermal dissociation				SID On C_{18} surface			SID on fluorinated surface		
Process	T (K)	k (s^{-1})	E_a (kcal/mol)	Log A (log s^{-1})	E_{coll} (eV)	k (s^{-1})	T_{eff}[a] (K)	E_{coll} (eV)	k (s^{-1})	T_{eff}[a] (K)
$MH^+ \rightarrow$ fragments	608	81	38.3	15.7	15	8.2E3	713	5	3.7E4	755
	625	200			27.3[b]	1.4E5	796	13.4[c]	1.2E5	791
	653	730			40	4.8E5	838	25	5.9E5	846
$M_2H^+ \rightarrow MH^+ + M$	503	42	46.5	21.7	10	1.3E4	579	10	1.2E4	577
			±4.3[c]	±1.9[c]						
	513	122			14.1[b]	1.3E5	613	11.4[c]	2.1E5	621
	521	215			18	4.8E5	635	18	2.9E5	626
$M_2H^+ \rightarrow$ fragments					55	3.5E4		25	2.1E4	
					65[b]	8.8E4		40.8[c]	1.8E5	
					80	3.8E5		55	6.6E5	

[a] Effective temperature calculated from $k = A\exp(-E_a/RT)$, applying the thermal kinetic parameter to the SID dissociation rate constants.
[b] Inflection point of the SID fragmentation efficiency plots.
[c] Average and sample standard deviation calculated from five replicate measurements.

greater than the decomposition rate, suggesting limiting high-pressure kinetics.[21]

As to the thermalization of the carrier gas itself, computer models[22] show that at our flow rates the air reaches 97.5% of the wall temperatures in 10 cm. Therefore, we used a total heated zone of 18 cm, and considered reaction onset after 10 cm. To test gas thermalization, we also used a reactor tube with a length of 30 cm, which allows thermalization through a longer flow zone. We obtained similar results with the two reactors, suggesting that further thermalization of the gas did not have any observable effect. Since the temperature dependence in the decomposition range is very sharp, as shown below, this observation suggests that the gas is already thermally equilibrated in the shorter reactor.

Also in our set-up, an additional 5 cm of tubing at the entrance electrospray tip is exposed to ambient air and remains at a constant temperature of approximately near 300 K, assuring that the observed decomposition temperature effects are not due to electrospray conditions. However, a weaker temperature effect is observed below the decomposition temperatures, which actually leads to increasing dimer production with increasing temperatures. This may be attributed to faster desolvation at the entry to the reactor tube, leading to more concentrated droplets which would facilitate the production of more adducts[23] (see below). The trend may be also due to faster diffusion of the monomer vs. dimer to the wall at higher temperatures.

With these instrumental parameters, we observed protonated monomer and dimer ions obtained by electrospraying a solution of 180 nmol leucine enkephalin per mL of 9:1 acetonitrile:water through a 1 cm gap with a voltage of 3.4 kV. The monitored monomer, dimer, and trimer peaks are shown in Fig. 3 at three different temperatures. Note that at low temperature (277 K, Fig. 3(a)), even the timer is observed, and more monomer than at a temperature of 483 K, (Fig. 3(b)). With increasing temperature, the intensity of the dimer increases slightly at first (see Fig. 3(b)) and then drops; and at 537 K, the monomer dominates. To illustrate the processes in a wider temperature range, the dimer/[monomer + dimer] ratio as a function of temperature is shown in Fig. 4. At lower temperatures, only a slow change is observed, possibly due to desolvation effects as noted above. These effects level off at about 400 K. However, from 490 to 530 K, the dimer intensity drops sharply and disappears. The sharp decomposition is similar to ion pyrolysis behavior studied previously in smaller model systems.[1-4]

Similarly, the monomer ion intensity of $(YGGFL)H^+$ also decreases rapidly over a short temperature range at higher temperatures. In both the monomer and dimer decompositions, the observed lower-mass decomposition product intensities do not fully compensate for the intensity loss of the decomposing ions. We attribute this to faster loss of the product lower-mass ions by diffusion to the capillary walls. For this reason, the (parent + fragment) intensity cannot be used (as I_0) to normalize the reactant ion intensity for calculating the rate constant from $\ln(I/I_0) = -kt$. Rather, we used internal standards that are stable against decomposition over the observed range. We found that the sodium complex $(YGGFL)Na^+$, and the

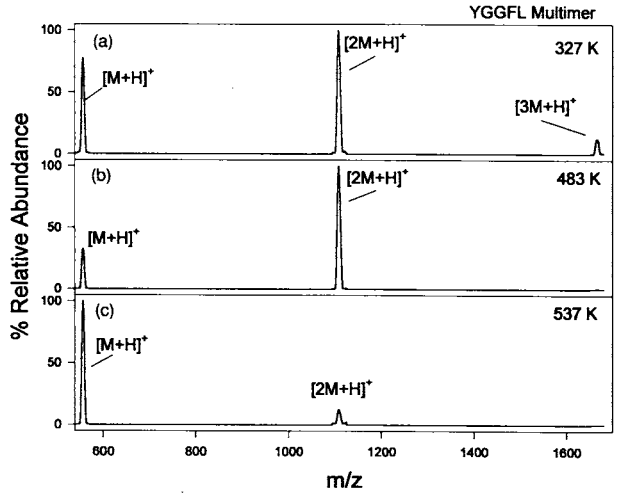

Figure 3. ESI mass spectra of leucine enkephalin obtained at (a) 327 K, (b) 483 K, and (c) 537 K external capillary temperature. After determining that no ions were present except M_nH^+ ($n = 1$–3) in this temperature range, to improve ion signal and to decrease the total scan time, scan windows of m/z 540–570 (monomer), 1090–1120 (dimer) and 1650–1680 (trimer) were used to selectively monitor the ions of interest.

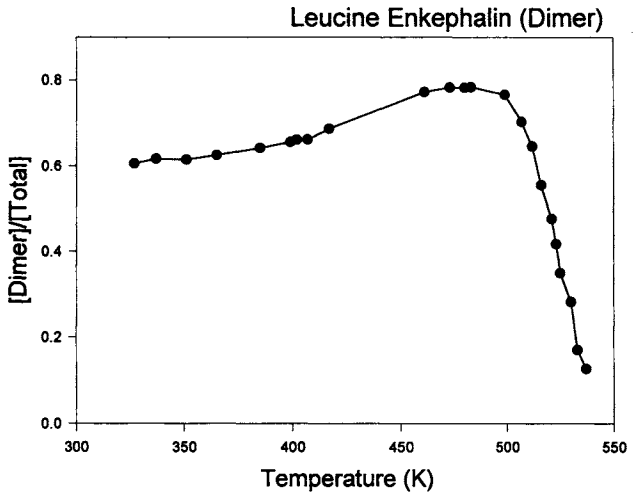

Figure 4. Normalized intensity of the $(YGGFL)_2H^+$ dimer as a function of temperature of the external capillary.

modified analogue $(YGGFL-Arg)H^+$ were suitable stable ions as internal standards over the temperature range of interest. Accordingly, we calculated the rate constant from $\ln[(I(MH^+)/I(B^+)_T/I((I(MH^+)/I(B^+))_{T_0}] = -kt$, where $I(B^+)$ is the intensity of the reference ion and T_0 is a low temperature where fragmentation is not significant.

The kinetic data for the decomposition of $(YGGFL)H^+$ are shown in the Arrhenius plot in Fig. 5. The data give an activation energy of 38.3 kcal/mol and a pre-exponential factor of log A = 15.7, similar to the typical value for unimolecular dissociations for log A of about 16. We also note that the present decomposition is observed at high temperatures of 360–400 °C due to the short, millisecond time-scale of the experiments. A thermal decomposition on the typical laboratory time-scale of, for example, 1 h, requiring $k = 2.8 \times 10^{-4}\ s^{-1}$, with the present Arrhenius parameters would require a temperature of 163 °C, a reasonable temperature for pyrolizing a polymer.

In relation to the thermal dissociation of the dimer ion $(YGGFL)_2H^+$, we have used the intensity data from a set of experiments to obtain rate coefficients for

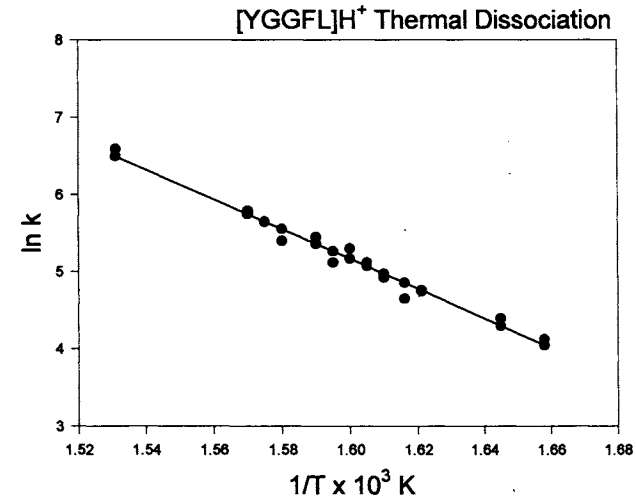

Figure 5. Arrhenius plot (ln k vs. $1/T$) for the thermal fragmentation of the $(YGGFL)H^+$. The calculated activation energy and log A factor are 38.3 kcal/mol and 15.7, respectively.

the dimer dissociation. An Arrhenius plot based on these data gives $\log k = 21.7 \pm 1.9 - 46.5 \pm 4.3/RT\ s^{-1}$, where the activation energy is expressed in kcal/mol. It is noted that the reaction occurs over a narrow temperature range, which causes substantial error margins in the Arrhenius parameters. For this reason, we replicated the temperature study six times, and the results shown are the average values, where the associated uncertainty in the rate expression is calculated to one standard deviation, reflecting the scatter in the Arrhenius plot. Note that such a high A factor can be attributed to a high-entropy transition state, which could form in the dissociation process of oligopeptide dimers. It is noted that the A factor for monomer fragmentation above was lower (log A = 15.7). By assuming a 'usual' log value of 16 for the dimer dissociation, combined with the measured rate constant, for example, $k(507\ K) = 24.5\ s^{-1}$, this would give an E_a of 34 kcal/mol for leucine enkaphalin dimer dissociation. (We applied a similar approximation to the dissociation of the dimer ion of a model alanine derivative $(CH_3CONHCH(CH_3)COOCH_3)_2H^+$ and also obtained a value of 34 kcal/mol, which is near the binding energy obtained from equilibrium studies of 30.1 kcal/mol.[24])

Note that at the high pressure limit, the activation energy may be equated with the energy barrier to decomposition. This may be equated tentatively with the dimer binding energy, assuming no significant reverse barrier, as may be expected for the dissociation of non-covalent hydrogen-bonded complexes. The strong binding energy observed would be similar to those observed in polydentate hydrogen bonded complexes such as protonated amines with polyethers, which show binding energies up to 45 kcal/mol.[24]

Relation between thermal and SID dissociation

The extent of decomposition following activation by surface collision can be used to calculate the dissociation rate constants. The Arrhenius activation parameters can then be used to assign an effective temperature to the ions, at which equal dissociation rate constants would apply. Finally, if the partition functions of the ions are known, the effective temperature can be used to calculate the average internal energy of the ions, and comparing this with the collision energy yields the energy deposition function.

For example, the observed normalized dimer intensities from the fragmentation efficiency curve for the dissociation of the leucine enkephalin dimer ion yields $\{\ln(I(\text{dimer})/(I(\text{monomer}) + I(\text{dimer})) = -kt\}$. By using a transit time from the collision surface to entry into the analyzing quadrupole as an average of 5×10^{-6} s in our instrument, we calculate rate constants in the range of $2\text{–}48 \times 10^4\ s^{-1}$ at collision energies of 10–20 eV as shown in Table 1. The Arrhenius parameters obtained above can then be used to assign effective temperatures of 580–630 K to the dimer ions activated at the above collision energies (Table 1). As described above, this can be used to assign internal energies and energy deposition efficiencies once the partition functions for the peptides are known. The determination of partition functions requires further approximations and these studies are beyond the scope of the present paper.[25]

It is shown in Fig. 6(a) and (b) that protonated

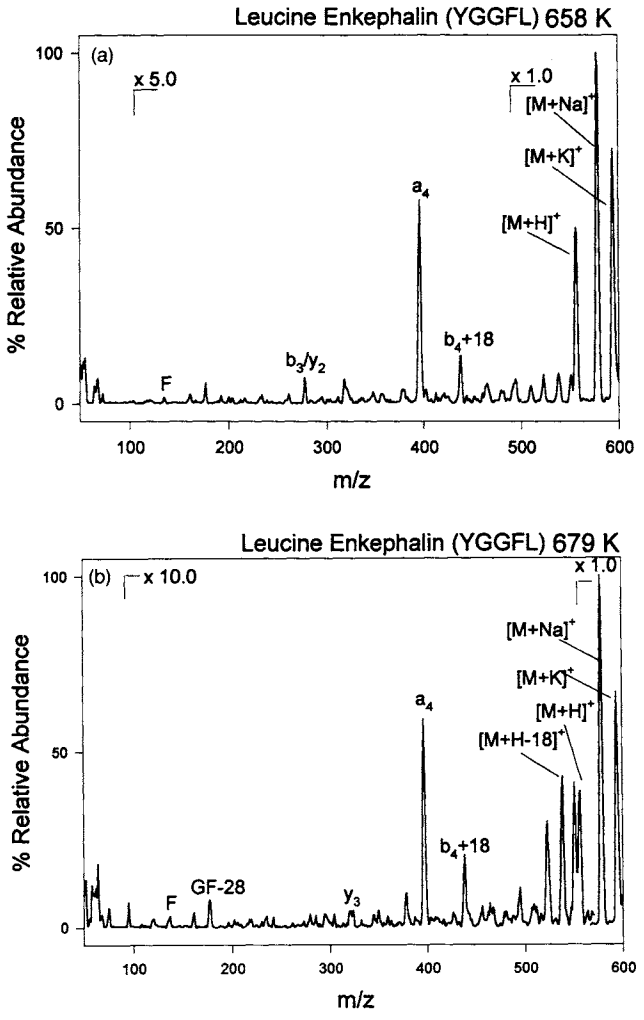

Figure 6. Thermal decomposition spectra of protonated leucine enkephalin at (a) 658 K and (b) 679 K.

leucine enkephalin fragments thermally. The comparison with the SID spectra obtained for both the monomer (Fig. 1(a)) and dimer (Fig. 1(b)) shows that there are significant differences in fragment ion intensities. The most relevant example is the intense peak at *m/z* 398 (which corresponds to the $\mathbf{a}_4$ fragment ion) in thermal dissociation spectra. It was possible to obtain an Arrhenius plot and to calculate the activation parameter for the overall fragmentation process as $E_a = 38.3$ kcal/mol, $\log A = 15.7$. Using these values, the effective temperatures of the SID activated ions for the fragmentation of $(YGGFL)H^+$ can be assigned as shown in Table 1. It is promising that comparisons can be made of fragmentation processes occurring over different time-scales and activation mechanisms.

Figure 7(a)–(c) compares the SID and thermal dissociation of melittin. The kinetics of the thermal decomposition were studied by Busman *et al.*[5] These thermal processes occur at considerably higher temperatures than the fragmentation of leucine enkephalin (810–840 K vs. 640–680 K). The pattern of the fragment ions obtained at 840 K is similar to that obtained by 135 eV SID of the triply charged melittin $[M + 3H]^{3+}$ on the fluorinated surface. (Note that at slightly lower temperature, *ca.* 810 K, the quadruply charged molecular ion, which is very intense at even lower temperatures (Fig. 7(b)), disappears and the triply charged ion and its fragments are predominant in the thermal spectrum in the range of 810–840 K). The appearance of a relatively large number of fragment ions with considerably intensity in the thermal dissociation spectra of melittin indicate that direct thermal dissociations can be useful for analytical purposes, i.e., for sequencing peptides.

The results reflect two basic differences between thermal and surface activation. First, the thermal dissociation emphasizes low-energy processes, since once activated for these processes, decomposition will occur before higher activation is possible, whereas in single gas-phase or surface collision activation, high energies are deposited in one collision making more energetic processes competitive. Second, if a high-energy decomposition can be followed by a lower-energy process, the subsequent fragmentation is always expected to occur in thermal systems, because the first fragment is rapidly reactivated. In comparison, in single-collision activation, the products of the first process can carry away enough energy to make the second step unfeasible. Therefore, thermal decomposition is not expected to yield **b** ions, but to proceed to the **a** ions through the low energy CO loss process, as is shown by the $(YGGFL)H^+$ spectra.

CONCLUSIONS

In the present paper, we have demonstrated that thermal decomposition studies, using a simple instrumental modification of standard electrospray aparatus, can give useful information on protein dissociation kinetics and possibly binding energies. This could be especially useful if non-specific and specific adducts turn out to have different binding energies and can be distinguished on this basis. The thermal binding energies can be used to estimate 'effective temperatures' of activated ions from the surface-induced dissociation rate constants. In turn, the effective temperatures can be used in the future to calculate the internal energies of the activated ions, if partition functions of the ions are known with reliable accuracy. From the relation between the collisional and internal energies, the energy deposition efficiency can be calculated.

A possible important application of thermal dissociation may be dissociation of covalent protein ions at high temperatures. This is illustrated by the dissociation of the $(YGGFL)H^+$ ion, whose products show both interesting similarities and differences to SID dissociation. Such processes could yield information complementary to collisional activation (both CAD and SID) with simple and inexpensive apparatus. Moreover, the thermal studies can yield basic information such as the pre-exponential factors and activation energies for fragmentation reactions. These parameters can also be of analytical use as they should be dependent on structural factors. For example, the activation energies should be smaller for dissociation near residues with electron-donating groups that can stabilize the product ions. These studies are also of basic interest in chemical kinetics as they extend the quantitative study of unimolecular reactions to macromolecules with hundreds, or even thousands, of internal degrees of freedom. In the future, we will study the thermal dissociation both of protein ions and of non-covalent adducts to examine the thermal behavior and energetics of biopolymers.

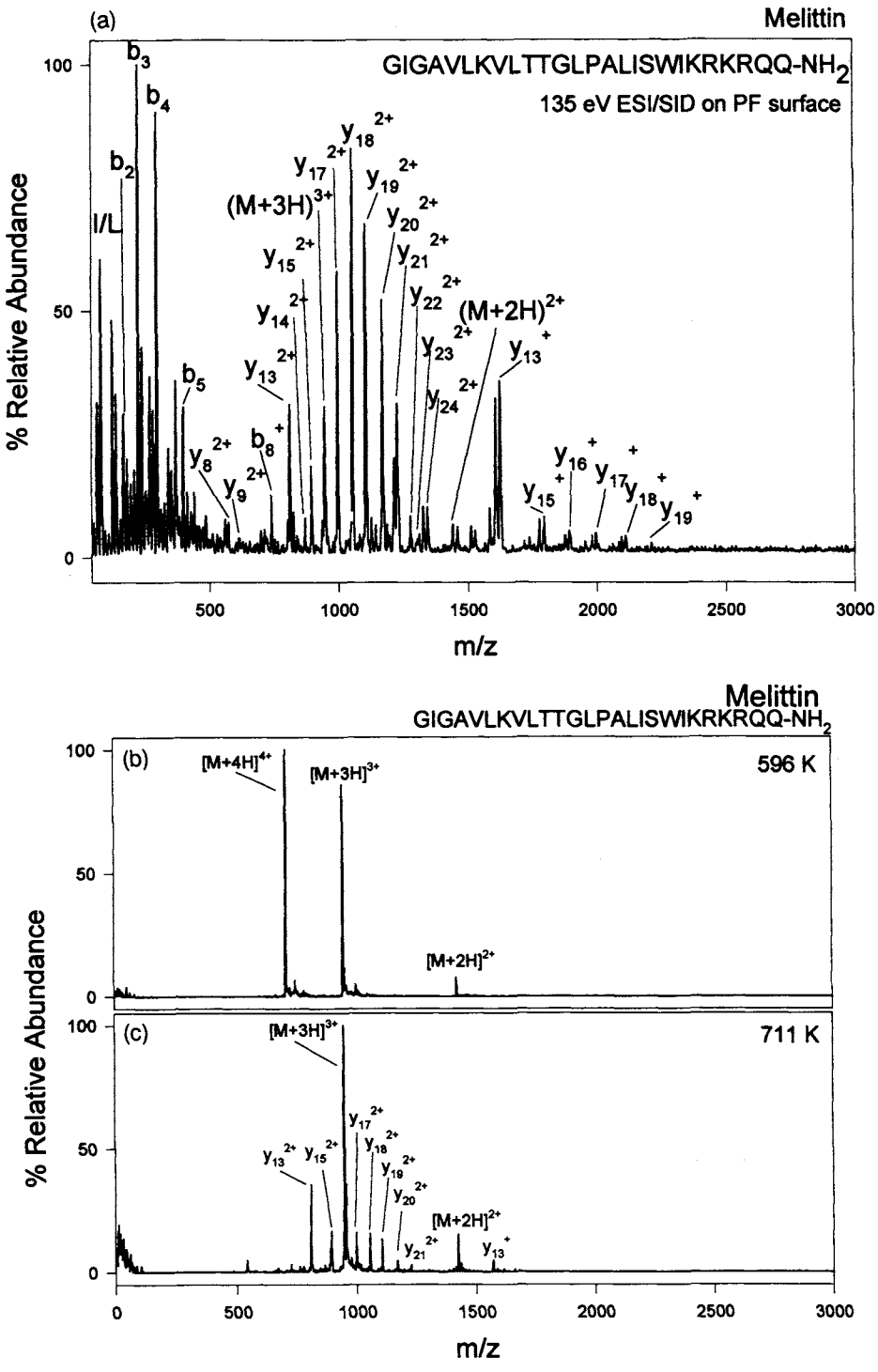

Figure 7. (a) Surface-induced dissociation spectra of triply charged melittin at 135 eV collision energy on the fluorinated surface. Thermal dissociation mass spectra of melittin at (b) 596 and (c) 711 K.

EXPERIMENTAL

The tandem mass spectrometer used in the present investigation has been described earlier.[15] The instrument consists of two Extrel 4000 u mass range quadrupoles positioned at 90°, with a surface placed to intersect the ion optical path at 45° to the incident ion beam. Self-assembled monolayer surfaces were prepared by the spontaneous assembly of 2-(perfluorooctyl)-ethanethiolate (F surface) and octadecanethiolate (C_{18} surface) on UV-cleaned, vapor-deposited gold. For further details and surface preparation, see Ref. 26. The surface holder designed originally for four surfaces[26] was used to guarantee a similar laboratory environment for both the F and C_{18} surfaces.

Protonated leucine enkephalin monomer and protonated dimer were generated by an electrospray source that was designed similarly to those described by Chowdhury *et al.*[27] Strong protonated dimer was formed by using a leucine enkephalin solution of 180 nmol/mL in 9:1 CH_3CN/H_2O. The water portion contained 1% acetic acid. The syringe was held at 3–4 kV and the capillary and skimmer voltages were kept at the same value (90 eV) to avoid gas-phase collision

activation in the capillary skimmer region. The surface potential was also held at 90 V for transmission of ions past the surface without collision (0 eV, or regular mass spectrometry). The collision energy was varied by lowering the surface potential to a selected value (e.g., 60 V for a 30 eV collision).

Thermal activation was accomplished in an external capillary added in front of the electrospray capillary leading into the mass spectrometer. The internal capillary had a diameter of 0.51 mm and was 45 cm in length. The external flow reactor capillaries had a slightly larger diameter of 0.76 mm. Two external capillaries with different lengths were used in this investigation. (One with a length of 25 cm and a heated zone of 18 cm, and another with a length of 40 cm and a heated zone of 30 cm). The external capillary was heated with a nichrome wire and the temperature measured with an iron–constantan thermocouple wrapped around the capillary. The assembly was wrapped in insulating tape to homogenize the temperature. Further considerations will be discussed in a future paper.[20]

Acknowledgement

This work was supported by a grant from the National Institute of Health (Grant: U.S. DHHS, 1R01GM51387).

REFERENCES

1. M. Meot-Ner (Mautner) and F. H. Yield, *J. Phys. Chem.* **80**, 2865 (1976).
2. M. Meot-Ner (Mautner) and L. W. Sieck, *Int. J. Mass Spectrom. Ion Processes* **92**, 123 (1989).
3. (a) L. W. Sieck and M. Meot-Ner (Mautner), *J. Phys. Chem.* **88**, 5324 (1984).
4. L. W. Sieck and M. Meot-Ner (Mautner), *J. Phys. Chem.* **88**, 5328 (1984).
5. M. Busman, A. L. Rockwood and R. D. Smith, *J. Phys. Chem.* **96**, 2397 (1992).
6. R. G. Cooks, T. Ast and Md. A. Mabud, *Int. J. Mass Spectrom. Ion Processes* **100**, 209 (1990).
7. R. A. Chorus, D. P. Little, S. C. Beu, T. D. Wood and F. W. McLafferty, *Anal. Chem.* **67**, 1042 (1995).
8. K. L. Shey, D. A. Durkin and K. R. Thornburg, *J. Am. Soc. Mass Spectrom.* **6**, 257 (1995).
9. D. Desperoux, A. D. Wright and K. R. Jennings, *Int. J. Mass Spectrom. Ion Processes* **126**, 95 (1993).
10. (a) W. Aberth, *Anal. Chem.* **62**, 609 (1990). (b) R. B. Cole, S. LeMeillour and J.-C. Tabet, *Anal. Chem.* **64**, 365 (1992). (c) J. A. Castoro, C. L. Wilkins, A. S. Woods and R. J. Cotter, *J. Mass Spectrom.* **30**, 94 (1995).
11. A. L. McCormack, J. L. Jones and V. H. Wysocki, *J. Am. Soc. Mass Spectrom.* **3**, 859 (1992).
12. A. L. McCormack, Á. Somogyi, A. R. Dongré and V. H. Wysocki, *Anal. Chem.* **65**, 2859 (1993).
13. (a) J. L. Jones, A. R. Dongré, Á. Somogyi and V. H. Wysocki, *J. Am. Chem. Soc.* **116**, 8368 (1994). (b) J. L. Jones, A. R. Dongré, Á. Somogyi and V. H. Wysocki (in preparation).
14. M. Morris, D. E. Riederer, Jr., B. E. Winger, R. G. Cooks, T. Ast and C. E. D. Chidsey, *Int. J. Mass Spectrom. Ion Processes* **122**, 181 (1992).
15. V. H. Wysocki, J.-M. Ding, J. L. Jones, J. H. Callahan and F. L. King, *J. Am. Soc. Mass Spectrom.* **3**, 29 (1992).
16. S. A. Miller, D. E. Riederer, Jr., R. G. Cooks, W. R. Cho, H. W. Lee and H. Kang, *J. Phys. Chem.* **98**, 245 (1994).
17. K. Vékey, Á. Somogyi and V. H. Wysocki, *J. Mass Spectrom.* **30**, 212 (1995).
18. V. H. Wysocki, H. I. Kenttämaa and R. G. Cooks, *Int. J. Mass Spectrom. Ion Processes* **75**, 181 (1987).
19. Based on the acronym of the author, relationship (1) may be denoted as the MAD SOW equation.
20. M. Meot-Ner (Mautner), A. R. Dongré, H. Nair, Á. Somogyi and V. H. Wysocki (in preparation).
21. W. Forst, *Theory of Unimolecular Reactions*, Academic Press, New York 1973.
22. T. Sebeci and P. Bradshow, *Physical and Computational Aspects of Convective Heat Transfer*, Springer-Verlag, Berlin 1984, p. 135 and Appendix.
23. J. B. Fenn, *J. Am. Soc. Mass Spectrom.* **4**, 524 (1993).
24. M. Meot-Ner (Mautner), *J. Am. Chem. Soc.* **105**, 4912 (1983).
25. One could make a rough comparison of the E_a obtained from the Arrhenius plot (46.5 kcal/mol) with the expected average internal energy deposited into the dimer for conversion to monomer, by multiplying the inflection point of the fragmentation efficiency curve by % conversion numbers obtained for small ions by the thermometer or deconvolution methods. This rough calculation leads to a value of 41 kcal/mol (assuming 13% conversion for the C_{18} surface). Although the values are strikingly similar, we hesitate to accept this oversimplified approach because of differences in the time scale and a lack of knowledge of the exact ln k vs. E curve.
26. Á. Somogyi, T. E. Kane, J.-M. Ding and V. H. Wysocki, *J. Am. Chem. Soc.* **115**, 5257 (1993).
27. (a) S. K. Chowdhury, V. Katta and B. T. Chait, *Rapid Commun. Mass Spectrom.* **4**, 81 (1990). (b) D. I. Papac, K. L. Schey and D. R. Knapp, *Anal. Chem.* **63**, 1658 (1991).